Cool white dwarfs as standards for infrared observations

Nicola Pietro Gentile Fusillo,[1]★ Pier-Emmanuel Tremblay,[1] Ralph C. Bohlin,[2]
Susana E. Deustua[2] and Jason S. Kalirai[3]

[1]*Department of Physics, University of Warwick, Coventry CV4 7AL, UK*
[2]*Space Telescope Science Institute, 3700 San Martin Drive, Baltimore, MD 21218, USA*
[3]*Johns Hopkins Applied Physics Laboratory, 11100 Johns Hopkins Road, Laurel, MD 20723, USA*

ABSTRACT

In the era of modern digital sky surveys, uncertainties in the flux of stellar standards are commonly the dominant systematic error in photometric calibration and can often affect the results of higher level experiments. The *Hubble Space Telescope* (*HST*) spectrophotometry, which is based on computed model atmospheres for three hot ($T_{eff} > 30\,000$ K) pure hydrogen (DA) white dwarfs, is currently considered the most reliable and internally consistent flux calibration. However, many next-generation facilities (e.g. Harmoni on E-ELT, *Euclid*, and *JWST*) will focus on IR observations, a regime in which white dwarf calibration has not yet been robustly tested. Cool DA white dwarfs have energy distributions that peak close to the optical or near-infrared, do not have shortcomings from UV metal line blanketing, and have a reasonably large sky density ($\simeq 4 \deg^{-2}$ at $G < 20$), making them, potentially, excellent calibrators. Here, we present a pilot study based on STIS + WFC3 observations of two bright DA white dwarfs to test whether targets cooler than current hot primary standards ($T_{eff} < 20\,000$ K) are consistent with the *HST* flux scale. We also test the robustness of white dwarf models in the IR regime from an X-shooter analysis of Paschen lines and by cross-matching our previously derived *Gaia* white dwarf catalogue with observations obtained with 2MASS, UKIDSS, VHS, and *WISE*.

Key words: line: profiles – stars: fundamental parameters – stars: individual: WD1327−083, stars: individual: WD2341+322 – white dwarfs – infrared: general.

1 INTRODUCTION

In the last 20 yr the advent of large area digital surveys revolutionized the way we observe the sky, and today astronomers can rely on terabytes of imaging data covering almost the entire sky from the ultraviolet (UV) to the infrared (IR). Modern electronic detectors allow a precision of <1 per cent in the determination of the physical energy distributions of stars and surveys like SDSS, PanSTARRS, and *Gaia* can boast internal relative photometric accuracies on the scale of 1–2 per cent (Padmanabhan et al. 2008; Chambers et al. 2016; Evans et al. 2018). However, any attempt to compare observations across different surveys and in particular across different wavelength coverage ultimately requires for all observations to be placed on a single reliable and consistent flux scale. The uncertainties in the flux of such absolute stellar standards are often the dominant systematic error in photometric calibration and propagate into the higher level analysis of several experiments.

For example our understanding of the nature of the dark energy, the driving force behind the observed accelerating cosmic expansion, fundamentally relies on the accurate comparison between the fluxes of Type Ia supernovae at different redshifts and therefore observed at different wavelengths (Riess et al. 1998; Perlmutter et al. 1999; Riess et al. 2000). Quantitative descriptions of dark energy in terms of the Einstein equations of general relativity are significantly improved when the relative flux with wavelength is known to an accuracy of 0.2 per cent or better (Scolnic et al. 2014). Currently, the most precise and internally consistent set of fluxes are the *Hubble Space Telescope* (*HST*) spectrophotometry, primarily from STIS and NICMOS, which are based on computed model atmospheres for three hot ($T_{eff} > 30\,000$ K) hydrogen atmosphere (DA) white dwarfs, GD71, GD153, and G191-B2B (Bohlin, Gordon & Tremblay 2014). The absolute flux at 5556 Å is fixed by ground-based measurements adjusted slightly to match MSX IR absolute fluxes (Bohlin 2014), but the relative flux at other wavelengths is entirely determined by the three hot white dwarf standards. Recent studies have largely confirmed the internal consistency of such calibration procedure with fainter secondary hot white dwarf standards (Narayan et al. 2019). Thus, our understanding of

★ E-mail: nicola.gentilefusillo@eso.org

cosmology and the nature of the dark energy is tied to the precision of model spectral energy distributions (SEDs) of hot white dwarfs.

There is a reassuring internal consistency of $\simeq 1$ per cent between the predicted hot white dwarf SEDs and the *HST* flux scale in the optical range (3500–8500 Å). However, other optical photometric surveys such as *Gaia*, PanSTARRS, and SDSS do not directly rely on the *HST* flux scale, resulting in a mismatch of white dwarf parameters when relying on different fitting techniques (Tremblay et al. 2019). Independent verifications of white dwarf fluxes are thus still needed to confirm the accuracy of the *HST* flux scale and improve the calibration of external photometric surveys. Such task is challenging and in this work we focus in particular on cooler and redder hydrogen-atmosphere white dwarfs. This aims at enhancing the accuracy of the *HST* flux scale and providing insight on the near- and mid-IR calibration regimes that have not been robustly tested with white dwarfs.

Many of next-generation facilities which will see first light in the next decade will focus on IR observations. The first-generation instrument HARMONI on E-ELT will be the telescope's workhorse for spectroscopy covering the wavelength range 0.47–2.45 µm (Thatte et al. 2016). The Euclid spacecraft will survey 15 000 deg^2 of the sky targeting hundreds of thousands white dwarfs as faint as 24 mag and the NISP instrument will provide near-IR photometry in *Y*, *J*, *H* bands, and low-resolution spectroscopy between 0.92 and 1.85 µm (Racca et al. 2016). The array of instruments on the *James Webb Space Telescope* (*JWST*) will carry out photometric and spectroscopic observations both in the near- and mid-IR regime down to 30 mag allowing to target the faintest and coolest white dwarfs even at the edge of the Milky Way (Kalirai 2018). Additionally, uncertainties in white dwarf fluxes are currently dominant in using the *Wide Field InfraRed Survey Telescope* (*WFIRST*) to precisely constrain the nature of dark energy (see fig. 9 of Hounsell et al. 2018). It is therefore of paramount importance to define precise flux standards in this wavelength regime. Hot white dwarfs have a low sky density ($\simeq 0.75$ deg^{-2} at $G < 20$) and their model atmospheres suffer from uncertainties due to non-local thermal equilibrium (NLTE) effects and the presence of metal traces and UV line blanketing (Giannias et al. 2010). Consequently, *HST*'s spectrophotometric white dwarf standards may not be ideal comparison objects for IR observations; and other types of white dwarfs or stars could be used as near-IR flux calibrators (Bohlin et al. 2014). However, recent WFC3 near-IR observations of hot white dwarfs are in good agreement with the *HST* flux scale (Narayan et al. 2019).

Following upon the preliminary analysis of Tremblay et al. (2017), here we test whether DA white dwarfs cooler than current hot primary standards ($T_{\rm eff} < 20\,000$ K) are consistent with the *HST* flux scale. Cool H-atmosphere white dwarfs have largely featureless energy distributions that peak in the optical or near-IR, and their colours are more similar to those of high-redshift supernovae or galaxies. Cool white dwarfs do not have shortcomings from NLTE effects or UV metal line blanketing, have a reasonably large sky density ($\simeq 4$ deg^{-2} at $G < 20$), and are generally closer than their hot counterparts, thus resulting in less or negligible reddening. In contrast, as white dwarfs cool below $T_{\rm eff} \approx 13\,000$ K they develop convective atmospheres that affect the measurement of their stellar parameters. State-of-the-art grids of 3D model atmospheres can now reliably account for convective effects (Tremblay et al. 2013) as verified by *Gaia* (Tremblay et al. 2019). Cool H-atmosphere stellar remnants have therefore a strong potential as IR calibrators. We base our study on STIS + WFC3 and X-Shooter observations of a small sample of bright DA white dwarfs. We also review the empirical and predicted near- and mid-IR white dwarf Hertzprung–

Russell diagram by cross-matching the extensive *Gaia* white dwarf catalogue of Gentile Fusillo et al. (2019) with the Two Micron All Sky Survey (2MASS), the UKIRT Infrared Deep Sky Survey (UKIDSS), the Vista Hemisphere Survey (VHS), and the *Wide-field Infrared Survey Explorer* (*WISE*). This provides further insights on the accuracy of white dwarf models at these wavelengths.

2 HUBBLE SPACE TELESCOPE SPECTROPHOTOMETRY

2.1 STIS and WFC3 observations

In cycle 23, we obtained four orbits of STIS and WFC3 observations (GO-14213) of two intermediate temperature ($12\,500$ K $\lesssim T_{\rm eff} \lesssim 15\,000$ K) H-atmosphere white dwarfs: WD1327−083 and WD2341+322. We selected objects that were bright enough to achieve a 1 per cent flux precision similar to current hot standards (Bohlin et al. 2014) in two orbits. We have excluded ZZ Ceti pulsators ($10\,500$ K $\lesssim T_{\rm eff} \lesssim 12\,500$ K at log $g = 8.0$ (log g/[cm s^{-2}]), see Tremblay et al. 2015) and suspected binaries. We also exclude magnetic white dwarfs as these objects are known to show photometric and spectroscopic variability and have SEDs which are extremely challenging to model (e.g. Brinkworth et al. 2013). Finally, white dwarfs with trace metals (DAZ) were also discarded as possible targets. A small fraction of these stars are known to exhibit IR emission from a dusty debris disc (Becklin et al. 2005), which would make the target unsuitable for IR calibration. The selected targets are in the intermediate temperature regime between current hot white dwarf standards and cooler non-pulsating H-atmospheres ($T_{\rm eff} < 10\,500$ K). These objects are cool enough to have negligible NLTE effects and seemingly no metal opacity in the UV, yet they are not in the regime where 3D corrections due to convection are significant (Tremblay et al. 2013). In the future, we hope to secure similar *HST* observations for even cooler bright white dwarfs and in the meantime we will explore the calibration potential of cooler white dwarfs with existing photometric observations in Section 4.

STIS spectroscopy of our two stars with the G140L, G230L, G430L, and G750L gratings covers the range 1150–10 000 Å at a resolution of $R = 500$–1000. Our STIS spectrophotometry is augmented by WRC3 IR grism observations with coverage from 8000 to 17 000 Å using G102 and G141 with resolutions $R = 200$ and 150, respectively (Bohlin & Deustua 2019). The STIS data are processed with the updated calibration procedure of Bohlin, Deustua & de Rosa (2019), while details of the WFC3 grism calibration procedure appear in Bohlin, Deustua & Pirzkal (2015) and in Bohlin & Deustua (2019). The STIS and WFC3 SEDs are merged at 10 120 and 9700 Å for WD1327−083 and WD2341+322, respectively, to make complete *HST* SEDs for CALSPEC.[1]

2.2 Analysis

Setting up DA white dwarfs as flux standards generally implies first determining $T_{\rm eff}$, surface gravity (expressed as log g where g is in units of cm s^{-2}), radius, and reddening in order to define model absolute fluxes. The spectroscopic technique of fitting the observed Balmer lines with model SEDs (Bergeron, Saffer & Liebert 1992) has been widely regarded as the most precise method to determine $T_{\rm eff}$ and surface gravity of white dwarfs, which can then be converted

---

[1] http://www.stsci.edu/hst/instrumentation/reference-data-for-calibration-and-tools/astronomical-catalogs/calspec

Table 1. Previously published and newly calculated atmospheric parameters of the white dwarfs WD1327−083 and WD2341+322. All quoted uncertainties correspond to 1σ.

Method	WD1327−083		WD2341+322	
	$T_{\rm eff}$ (K)	log g	$T_{\rm eff}$ (K)	log g
Gianninas et al. ([2011](#), Balmer lines)	14 570 ± 240	7.99 ± 0.04	13 100 ± 198	7.92 ± 0.04
Gaia parallax + photometry (Gentile Fusillo et al. [2019](#))	14 861 ± 107	7.99 ± 0.01	12 650 ± 43	8.01 ± 0.05
STIS + WFC3 Balmer lines (Figs [1](#) and [2](#))	14 837 ± 406	8.01 ± 0.05	12 884 ± 214	8.06 ± 0.04
STIS + WFC3 continuum + *Gaia* parallax fit (Figs [1](#) and [2](#))	14 607 ± 290	7.99 ± 0.03	12 671 ± 330	8.02 ± 0.03
STIS + WFC3 Paschen lines (Fig. [6](#))	14 822 ± 830	8.00 ± 0.1	13 805 ± 840	8.05 ± 0.1

to radii using the well-understood white dwarf mass–radius relation. Relative uncertainties in these measurements are typically of the order of <2 per cent for high-signal-to-noise observations (S/N $\gtrsim$ 40; Liebert, Bergeron & Holberg [2005](#)) and are largely unaffected by reddening. The true accuracy of the atmospheric parameters is difficult to measure as it depends intimately on the accuracy of the line broadening physics (Tremblay & Bergeron [2009](#); Gomez et al. [2016](#)). However, absolute fluxes predicted by spectroscopy are in agreement with observed dereddened *Gaia* fluxes at a few per cent level (Genest-Beaulieu & Bergeron [2019](#); Tremblay et al. [2019](#)).

In contrast, white dwarf $T_{\rm eff}$ and radius can be determined by photometric analyses using broad-band colours and trigonometric parallaxes (Koester, Schulz & Weidemann [1979](#); Bergeron, Leggett & Ruiz [2001](#)). The advantage of this technique is that model fluxes for a given $T_{\rm eff}$ and radius are fairly robust because they depend on better known continuum opacities rather than line broadening physics. Furthermore, the recent *Gaia* DR2 provided a large sample of precise photometric and parallax measurements for white dwarfs allowing for relative $T_{\rm eff}$ and radius uncertainties that are now at the same precision level as spectroscopic analyses (Gentile Fusillo et al. [2019](#)). The drawback of this technique is that photometric measurements are subject to reddening and must be correctly calibrated to obtain reliable results. Currently, calibration issues appear to be the dominant uncertainty in using photometric solutions (Bergeron et al. [2019](#); Tremblay et al. [2019](#)). Photometric calibration is often performed by comparing with white dwarf parameters obtained by fitting spectroscopy (see e.g. Holberg & Bergeron [2006](#)), however, this approach does not necessarily allow for better accuracy in the atmospheric parameters.

Here, we use *HST* STIS + WFC3 spectrophotometry of two intermediate $T_{\rm eff}$ white dwarfs to compare different methods of estimating atmospheric parameters.

Our observations have been calibrated based on the current three hot white dwarf standards ($T_{\rm eff}$ > 30 000 K) in CALSPEC. Our targets have significantly lower $T_{\rm eff}$ values, hence have energy distributions that peak closer to the optical regime and that are not affected by continuum hydrogen opacities in the same way as hot white dwarfs. Therefore, they can serve as a test of the accuracy of the CALSPEC flux scale and possibly define on their own new primary standards.

We fitted the newly acquired STIS + WFC3 spectra of WD1327−083 and WD2341+322 using our grid of H-atmosphere models (Tremblay, Bergeron & Gianninas [2011](#); Tremblay et al. [2013](#)). The model atmospheres include Lyman, Balmer, Paschen, and Brackett line blanketing (40 lines in total) and use up to 1814 frequencies to solve radiative transfer for the atmospheric structures in the Rosseland optical depth range $-5 \lesssim \log \tau_{\rm R} \lesssim 3$. We use the non-ideal equation of state of Hummer & Mihalas ([1988](#)) both for populations and opacities (Tremblay & Bergeron [2009](#)). The grid spacing is given in section 2.2 of Tremblay et al. ([2011](#)).

We follow the standard spectroscopic fitting method by comparing continuum-normalized Balmer line profiles in the white dwarf spectra with our synthetic spectral models. Additionally, since STIS and WFC3 are spectrophotometrically calibrated, we also compare the entire STIS spectrum directly with our models without any normalization step. In this second procedure, we rely on the *Gaia* DR2 (Gaia Collaboration [2018](#); Gentile Fusillo et al. [2019](#)) parallax of the stars to scale the synthetic spectrum and directly fit the STIS flux to obtain a radius estimate. We then use the white dwarf mass–radius relationship (Fontaine, Brassard & Bergeron [2001](#)) to derive masses (0.61 ± 0.01 and 0.62 ± 0.02 M$_\odot$ for WD1327−083 and WD2341+322, respectively) and log g values for the stars and compare with the spectroscopic solutions. The models which best match the entire SED of the two white dwarfs are provided with the electronic distribution of this article. As shown in Table [1](#) the $T_{\rm eff}$ and log g values obtained using both methods are in excellent agreement (<1σ). The fact that these two fitting routines produce results in such good agreement indicates that the STIS + WFC3 spectra are not affected by interstellar reddening. Indeed no reddening should be expected for stars as close as WD1327−083 and WD2341+322 (16.1 and 18.6 pc, respectively).

Stellar parameters for these white dwarfs have also previously been published in Gianninas, Bergeron & Ruiz ([2011](#)) using independent spectroscopic observations and in Gentile Fusillo et al. ([2019](#)) using *Gaia* observations only. For WD1327−083, we find that our best solution closely agrees (<1σ) with both previously published values. For WD2341+322, our model analysis of the STIS spectrum results in parameters which are in excellent agreement with those from Gentile Fusillo et al. ([2019](#)), but are 2σ discrepant from the Gianninas et al. ([2011](#)) solution (Table [1](#)).

We have used our own grid of model atmospheres, but to our knowledge other grids of H-atmosphere white dwarfs use the same constitutive physics in this temperature range. Tremblay et al. ([2011](#)) show that their code fully connects with TLUSTY (Hubeny & Lanz [1995](#)), which is used at higher temperatures and Tremblay et al. ([2017](#)) have verified that the model atmosphere code of Koester ([2010](#)) provides similar spectroscopic and photometric solutions within 1σ for WD 1327−083. The systematic uncertainties from subsets of the input physics (e.g. line profiles) may be larger than the difference between the codes, but that is difficult to quantify.

Figs [1](#) and [2](#) clearly illustrate that, overall, our models successfully predict the observed STIS and WFC3 fluxes to within 3 per cent over most of the range between 1500 and 17 000 Å. In particular, in the near-IR between 8000 and 16 000 Å the model and observed fluxes diverge by less than 2 per cent for both white dwarfs. Overall our results suggest that there is no fundamental reason to limit white dwarf calibrators to $T_{\rm eff}$ > 20 000 K (Narayan et al. [2019](#)). Using a lower temperature limit would represent a five-fold enhancement in the sky density of white dwarf calibrators.
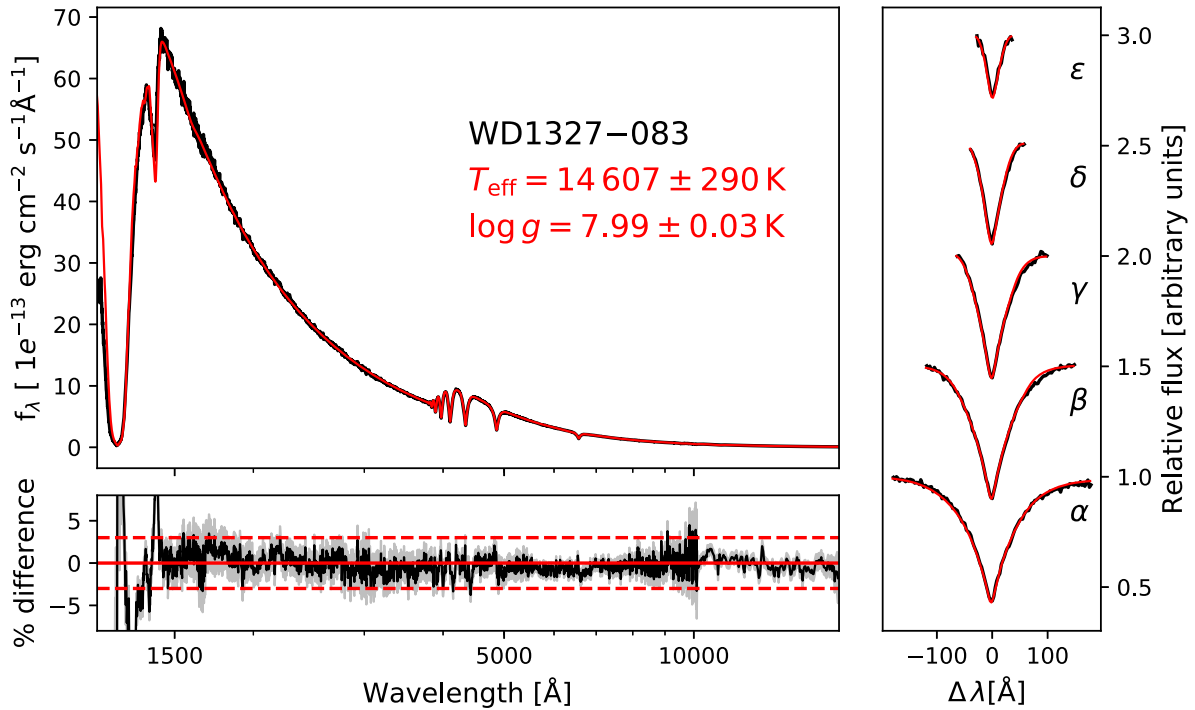
Figure 1. *Main panel*: STIS + WFC3 spectrophotometry of the white dwarf WD1327−083 with the best-fitting model and best-fitting parameters displayed in red. *Bottom panel*: Residuals in the difference between the observed flux and the model predicted flux. Uncertainties in the STIS + WF3 observed flux are represented by the grey-shaded region. The red dashed lines indicate the 3 per cent level. *Right-hand panel*: Best model fit to the Balmer lines. The line profiles are vertically offset for clarity. The best-fitting parameters are found in Table 1.
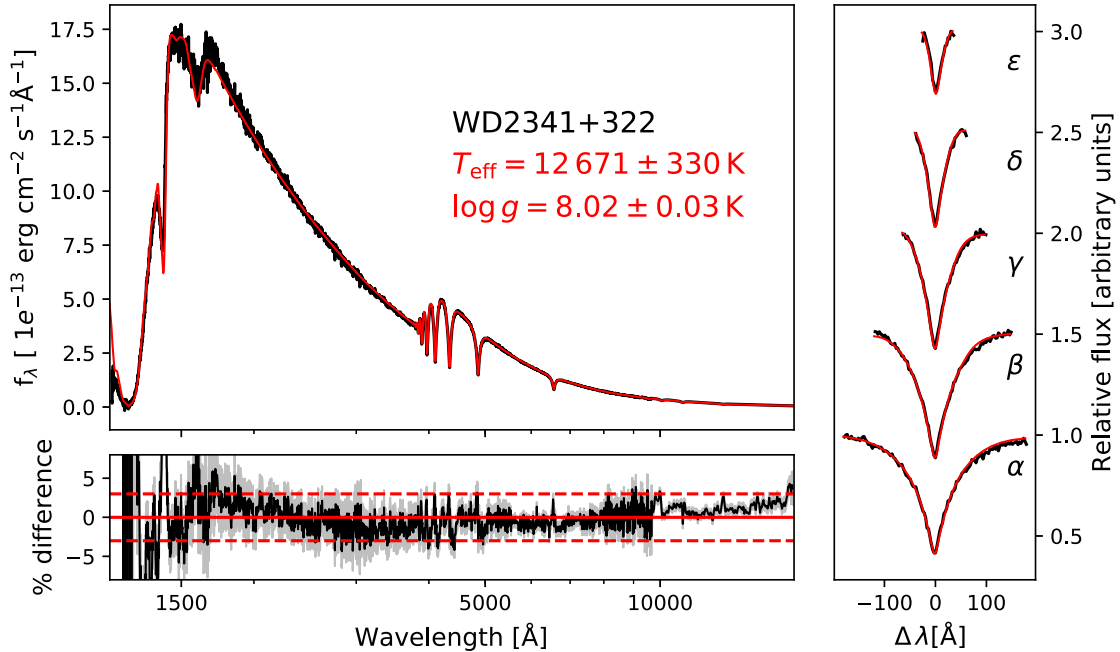
Figure 2. Similar to Fig. 1 but for STIS + WFC3 spectrophotometry of the white dwarf WD2341+322.

3 PASCHEN SERIES FITTING

The so-called spectroscopic method, which relies on comparing observed Balmer line profiles with model spectra, is widely regarded as a reliable technique to obtain $T_{\rm eff}$ and $\log g$ for H-atmosphere white dwarfs. In the near-IR between 8500 and 13 500 Å, the spectra

of white dwarfs display absorption features from the lower energy Paschen series. These line profiles can also be compared with model spectra and could in principle have the same diagnostic potential as Balmer lines. Testing whether current white dwarf model atmospheres correctly replicate observed Paschen line pro-

Table 2. Atmospheric parameters of the white dwarfs observed with X-shooter on the VLT. All quoted uncertainties correspond to 1σ.

Name	Balmer lines fit		Paschen lines fit	
	T_{eff} (K)	$\log g$	T_{eff} (K)	$\log g$
WD1229−012	20380 ± 385	7.57 ± 0.05	19450 ± 610	7.51 ± 0.1
WD1241−010[a]	24696 ± 265	7.41 ± 0.06	24561 ± 430	7.51 ± 0.1
WD1244−125	13254 ± 357	7.97 ± 0.04	12990 ± 800	8.01 ± 0.06
WD1310−305	20315 ± 317	7.91 ± 0.05	19590 ± 610	7.90 ± 0.07
WD1356−233	9644 ± 150	8.27 ± 0.07	9818 ± 180	8.32 ± 0.1
WD1407−475	22668 ± 448	7.78 ± 0.06	25360 ± 730	7.69 ± 0.1
WD1418−088	8090 ± 153	8.29 ± 0.04	8178 ± 160	8.36 ± 0.07
WD1500−170	32591 ± 526	7.94 ± 0.05	35000 ± 990	7.73 ± 0.1

[a]Double white dwarf binary (Marsh, Dhillon & Duck 1995).

files and whether stellar parameters obtained by fitting these lines are compatible with spectroscopic fits using Balmer lines has two purposes. First of all, the capability of white dwarfs as infrared calibrators rests on the ability of the model atmospheres to fit the observed data. Secondly, in the next decade key instruments onboard facilities such as *JWST* and *Euclid* will have IR-only capabilities, and Paschen lines could offer unique diagnostic opportunities for observed H-atmosphere white dwarfs.

According to the Hummer & Mihalas (1988) formalism, interactions between neighbouring particles cause atomic energy levels to have a certain probability of being dissociated, and in such case the absorption of a photon results in a bound-free transition (so-called pseudo-continuum opacity) instead of a regular line transition. In warm H-atmosphere white dwarfs where Paschen lines are observed, these non-ideal effects are caused by the interactions of the H atoms with charged protons and electrons. As a consequence the higher Lyman, Balmer, and Paschen lines can be much weaker than expected from an ideal equation of state. Tremblay & Bergeron (2009) were the first to combine Stark broadening with a consistent implementation of line dissolution according to the Hummer & Mihalas (1988) model. The implementation of these improved Stark profiles has been extensively discussed for the Balmer lines (Tremblay & Bergeron 2009) and the Lyman lines (Preval et al. 2015). Here, we include for the first time Paschen line profiles calculated under the formalism of Tremblay & Bergeron (2009). While these models have not been used by our group before, we note that broad-band near-IR photometry is not impacted by the details of line broadening, and therefore previously available colour tables are unchanged.

We developed a fitting routine for the Paschen lines of H-atmosphere white dwarfs. In order to construct a sample of test objects, we obtained VLT X-shooter (Vernet et al. 2011) observations of 10 bright H-atmosphere white dwarfs. The spectra were acquired in period 97 between 2016 April and July utilizing nodding mode, a 1 arcsec slit aperture for the UVB arm. 0.9 arcsec for the VIS arm, and 1.2 arcsec for the NIR arm. Exposure times ranged between 190 and 1190 s. The spectra were reduced using the standard procedures within the REFLEX[2] reduction tool developed by ESO (Freudling et al. 2013). The combined UVB, VIS, and NIR arms of X-shooter cover the entire spectral range from $\simeq$ 3000 to 14 000 Å which allows fitting both the Balmer and Paschen sequences. The X-shooter targets spanned a broad range of T_{eff}, but our observations revealed that at $T_{\text{eff}} \lesssim 8000$ and $T_{\text{eff}} \gtrsim 40\,000$ K the Paschen absorption lines become too weak for any meaningful

model comparison. Because of this restriction, we were able to compare stellar parameters only for 8 of our 10 stars (Table 2).

Analogously to the well-established Balmer spectroscopic fitting method, our newly developed Paschen fitting routine requires to first normalize the continuum of the spectrum of the white dwarf and then compare the individual Paschen lines to model spectroscopy (Fig. 3). Ground-based spectroscopic observations of the Paschen lines suffer from heavy contamination by atmospheric absorption features. Telluric lines removal is therefore crucial in order to proceed with any model comparison. We used MOLECFIT (Smette et al. 2015) to remove tellurics, but despite the overall success in cleaning the spectra, the results are not uniform across all objects and some residuals still affect the spectroscopy of some our targets. Residuals in the telluric line subtraction can affect the shape of the Paschen lines as well as the continuum normalization step resulting in less accurate stellar parameters. In our model comparison, we only rely on the Pa ϵ, Pa δ, Pa γ, and Pa β lines. Though visible in some the spectra, the higher order lines are too weak for a meaningful comparison with the models and Pa α is completely hidden by atmospheric features and cannot be recovered.

Fig. 4 shows that we find a good overall agreement between the stellar parameters obtained from the Paschen and Balmer line fits, but some solutions are significantly discrepant ($>3\sigma$). The outlying objects have particularly strong telluric absorption features in their X-shooter spectra and the subtraction procedure could not fully account for them. We observe a possible trend indicating that, with increasing T_{eff}, Paschen lines fit return lower $\log g$ values compared to Balmer lines fit (Fig. 5). However, with only eight white dwarfs in the sample this trend is potentially only apparent because of the outlier nature of WD1500−170. This is the hottest white dwarf examined and so the object with the weakest Paschen lines in the sample, making it particularly susceptible to imperfect telluric removal. None the less this comparison illustrates that our models correctly predict the line profiles of Paschen lines within uncertainties and near-IR spectroscopy can be used to estimate the stellar parameters of H-atmosphere white dwarfs. Space-based spectroscopy would be best suited for this type of observations as it would be free from the limitations introduced by the presence of telluric lines. The combined STIS + WFC3 spectra of WD1327−083 and WD2341+322 show clear Paschen absorption lines and so provide an additional opportunity to further test the reliability of our white dwarf models. As shown in Table 1, the stellar parameters obtained from the Paschen fits (Fig. 6) are in good agreement with those obtained from the Balmer lines and continuum fits. However it is important to point out that due to the low resolution of the WFC3 near-IR spectra, the uncertainties in stellar parameters obtained from the Paschen lines are relatively high.
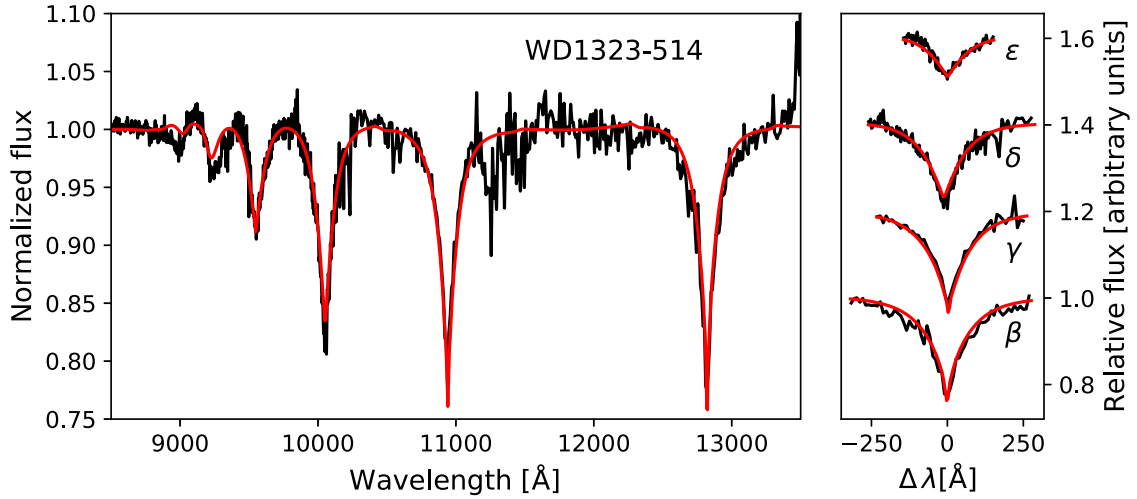
Figure 3. Atmospheric model fit to the Paschen lines from the telluric corrected, normalized, X-shooter spectrum of the white dwarf WD1323−514 (left-hand panel). Residuals from telluric line removal can still be seen between 12 000 and 13 000 Å. The individual lines used for the fit are displayed in the right-hand panel, vertically offset for clarity.
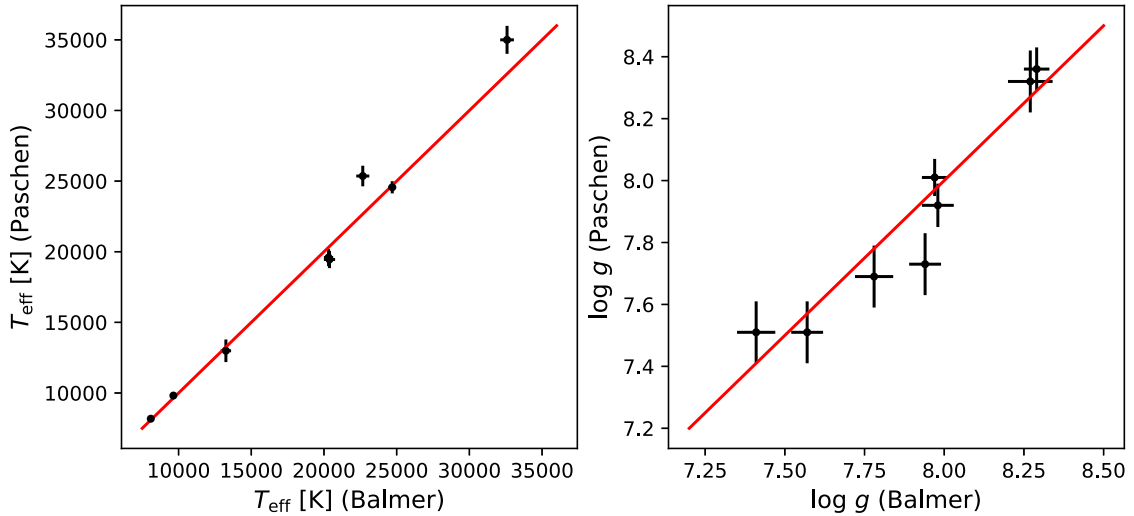

Figure 4. Comparison between T_{eff} (left-hand panel) and log g (right-hand panel) obtained by fitting Balmer and Paschen lines for eight bright H-atmosphere white dwarfs observed with X-shooter (see Table 2). The red lines represent the 1:1 relationship.

4 GROUND-BASED NEAR-IR AND WISE MID-IR PHOTOMETRY

Near-IR photometry can also be employed to test the accuracy of white dwarf models in this wavelength regime. While the calibration of ground-based photometric surveys may not be as well as understood as *HST* STIS and WFC3, the large number of observed white dwarfs, in many instances with the same object observed by two or more surveys, provides an advantage compared to the smaller *HST* data set. To date, a number of ground-based surveys provide near-IR photometric coverage in the *Y, J, H, K* bands, for vast areas of the sky. In this work, we focus on 2MASS, UKIDSS, and VHS as they provide the coverage of the largest number of white dwarfs.

2MASS covers the entire sky to a limiting magnitude of 15.8, 15.1, and 14.3 in *J, H*, and K_s, respectively. Nearly 20 yr after its nominal end, 2MASS remains a very powerful tool as the only all-sky near-IR survey (Skrutskie et al. 2006). None the less, the

relatively shallow magnitude depth limits the survey usefulness for intrinsically faint objects like white dwarfs.

UKIDSS is the collective name of a group of five near-IR surveys: the Large Area Survey (LAS), the Galactic Plane Survey (GPS), the Galactic Cluster Survey (GCS), the Deep Extragalactic Survey (DXS), and the Ultra Deep Survey (UDS). Because of its large footprint, UKIDSS LAS is best suited for our work. It provides imaging over 4000 deg² north of Dec. = −1.25 deg in four broadbands: *Y, J, H*, and *K*, with limiting magnitudes of 20.5, 20.0, 18.8, and 18.4, respectively (Lawrence et al. 2007).

VHS is the widest area near-IR survey conducted from the VISTA telescope at Paranal (Chile). It scans the sky in the *Y, J, H*, and K_s bands (McMahon et al. 2013) and the most recent data release (DR6) covers almost the entire Southern hemisphere.

Space-based observations in the mid-IR regime offer the opportunity to test white dwarf models at even longer wavelengths, but resources for large-scale comparisons are much scarcer compared
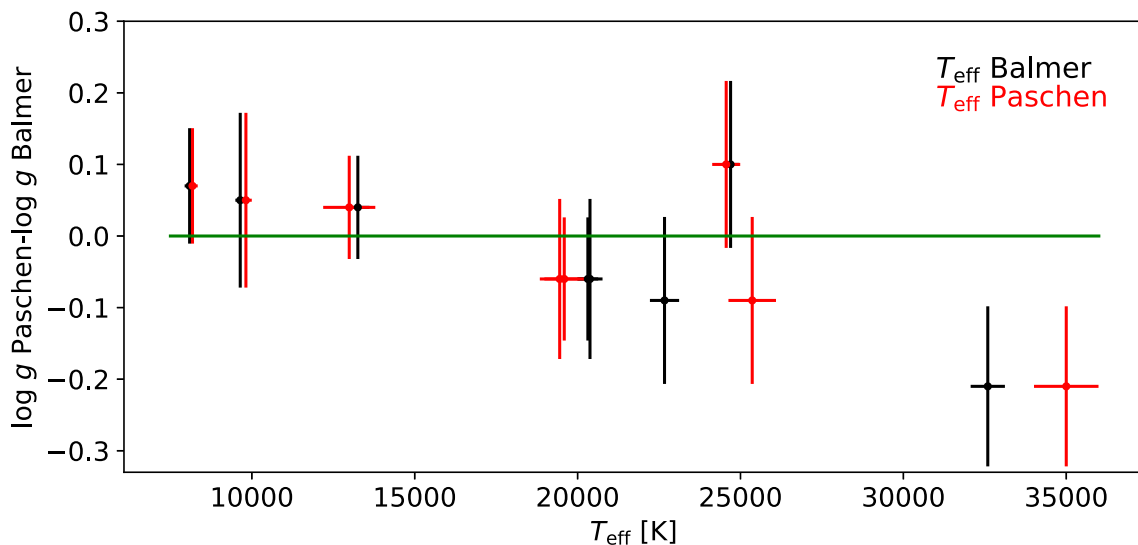
Figure 5. Comparison of the log g values obtained by fitting Paschen lines and Balmer lines, as a function of T_{eff}. Each object is included at the position of its T_{eff} value from Balmer lines fit (black) and from Paschen lines fit (red). The green horizontal line indicates the relationship log g (Paschen) = log g (Balmer).
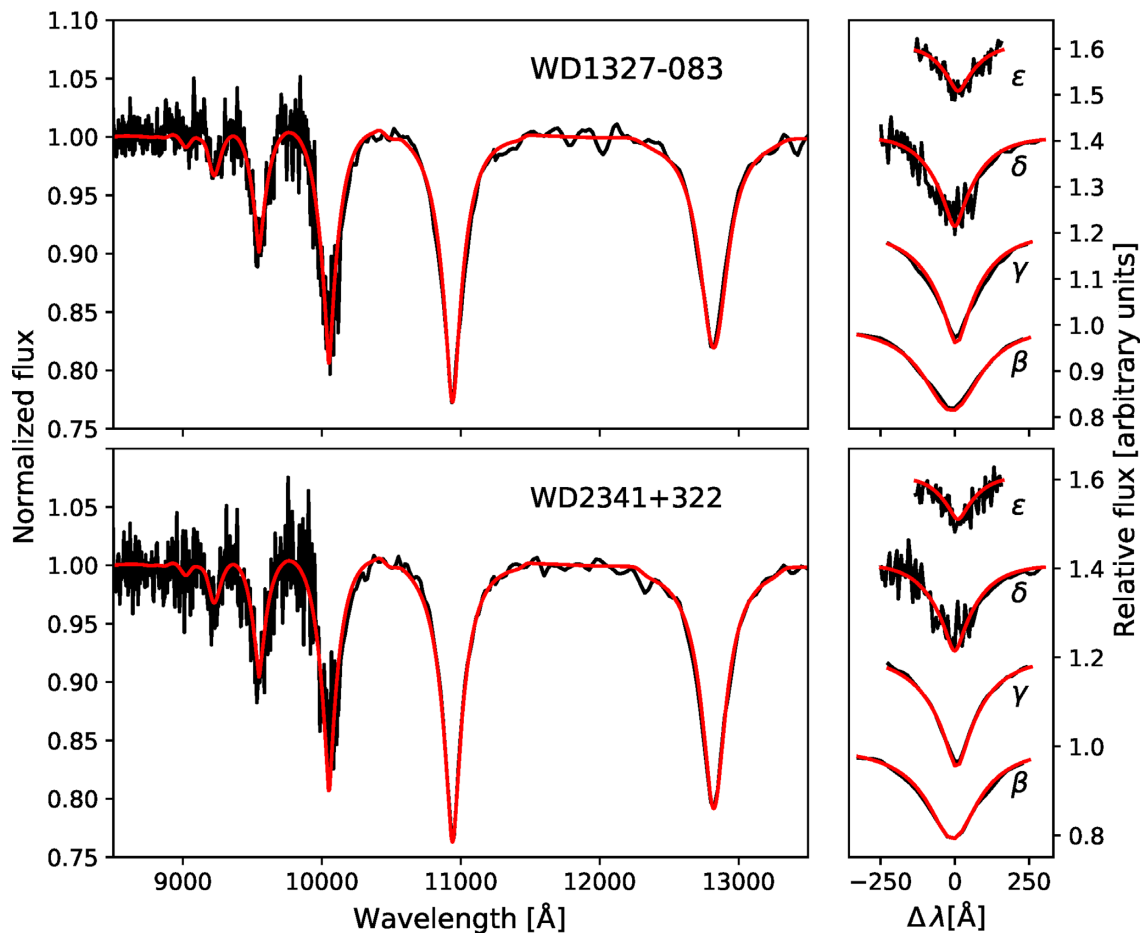

Figure 6. Atmospheric model fit to the Paschen lines from the STIS + WFC3 spectra of the white dwarfs WD1327−083 and WD2341+322. The individual lines used for the fit are displayed on the right-hand panels, vertically offset for clarity.

to the near-IR. The only reliable large-area survey in the mid-IR is *WISE*, which mapped the entire sky at 3.4, 4.6, 12, and 22 μm in four bands (*W*1, *W*2, *W*3, and *W*4; Wright et al. 2010). However, most white dwarfs only have reliable detection in the *W*1 band and

the low-spatial resolution of *WISE* (≃6 arcsec) makes large-scale cross-matching particularly challenging.

In order to compare IR fluxes predicted by current models with actual IR observations, we cross-matched the volume-limited
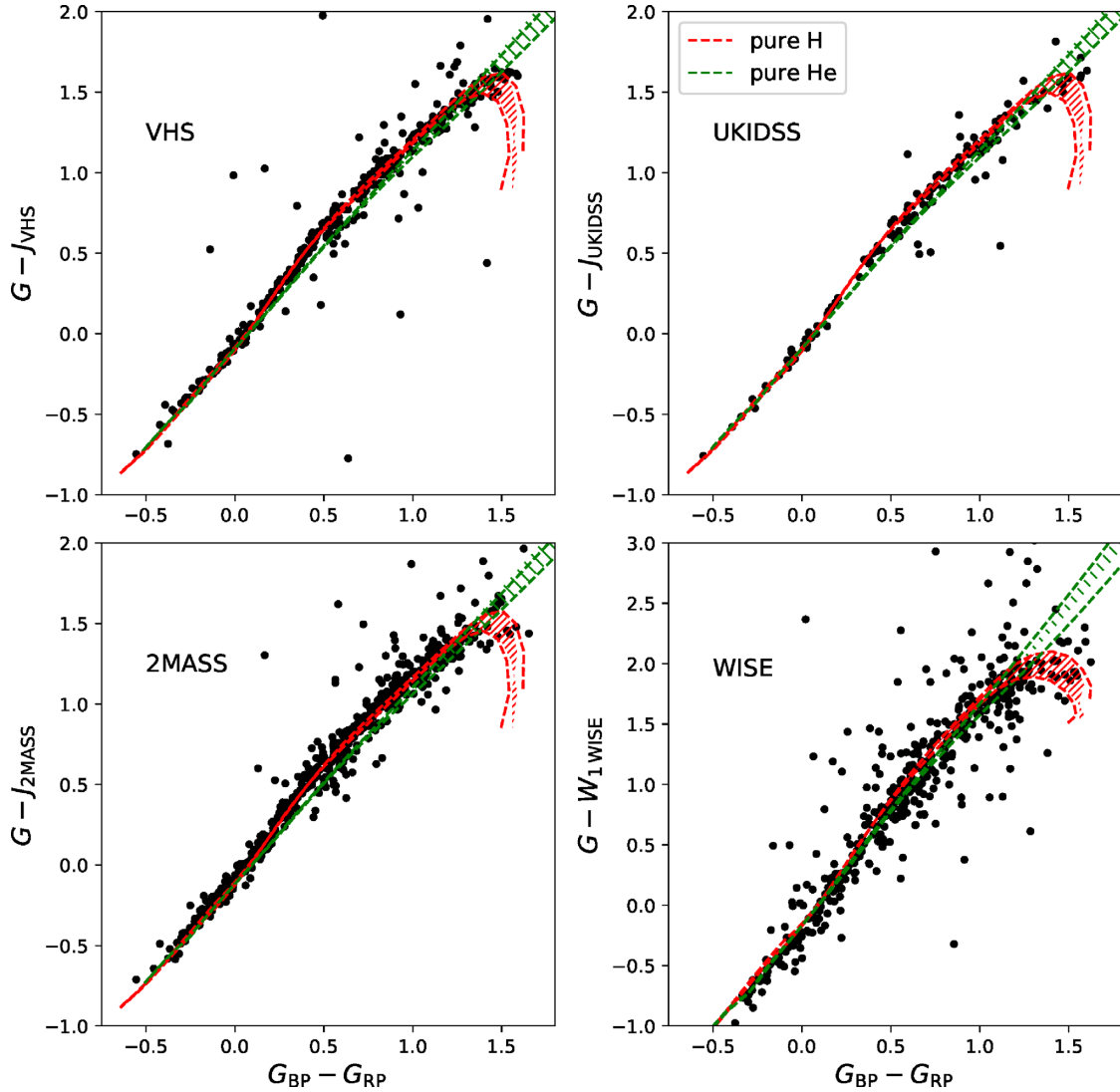
Figure 7. Colour–colour diagrams combining *Gaia G*, G_{BP}, and G_{RP} magnitudes with *J*-band measurements from VHS, UKIDSS, and 2MASS, and with *W*1 band from *WISE* for white dwarfs within 50 pc of the Sun observed by each survey. Cooling tracks for pure H and pure He atmosphere white dwarfs are displayed in red and green, respectively. The distribution of white dwarfs in these colour–colour spaces is mostly insensitive to log *g*. The shaded regions between the cooling tracks show the area spanned by objects with 7.5 < log *g* < 8.5. The predicted colours are in good agreement with the observed ones for all surveys.

50 pc sample of high-confidence white dwarf candidates ($P_{WD} \geq 0.75$) from the Gentile Fusillo et al. (2019) catalogue with the aforementioned four IR surveys. Given the relatively large wavelength difference between the Gaia *G* band and near-IR *J* bands, the comparison of the empirical and modelled $G - J$ colours can be a powerful tool to confirm the consistency of predicted model fluxes. The broad wavelength separation also means that $G - J$, $G - H$, and $G - K$ colours have very similar features but with decreasing precision, so for illustrative purposes we focus on $G - J$ (and $G - W1$ for *WISE*). The colour–colour diagrams in Fig. 7, using *Gaia* $G_{BP} - G_{RP}$ colour as an independent variable, clearly illustrate that the synthetic colours correctly match the observed white dwarf sequence in all four surveys. The larger scatter seen for *WISE* is caused by the relatively worse photometric data quality and potentially by a small number of mismatchings. The only significant difference between the photometric data and the models is the 'hook' due to collision-induced absorption in the pure hydrogen atmosphere tracks which appear not to be populated by any white

dwarf. The most likely cause is that the very cool ($T_{eff} < 4000$ K) white dwarfs which would occupy this area of the diagram are rare due to the finite age of Galactic disc, cool rapidly, and in most cases are too faint to be detected in the IR surveys. We note that such colour–colour diagrams have little sensitivity to surface gravity and even atmospheric composition as shown in Fig. 7, in clear contrast with the Hertzprung–Russell diagrams discussed in the next section.

4.1 IR Hertzprung–Russell diagrams

The top panels in Fig. 8 clearly illustrate the bifurcation, in the optical-colours Hertzprung–Russell diagram, between DA white dwarfs of typical surface gravity (top sequence) and the equivalent track of He-atmosphere white dwarfs (bottom sequence). Combining *Gaia* measurements with IR photometry also allows to inspect the H–R diagram distribution of white dwarfs in IR colour space. The bifurcation between DA white dwarfs and He-atmosphere
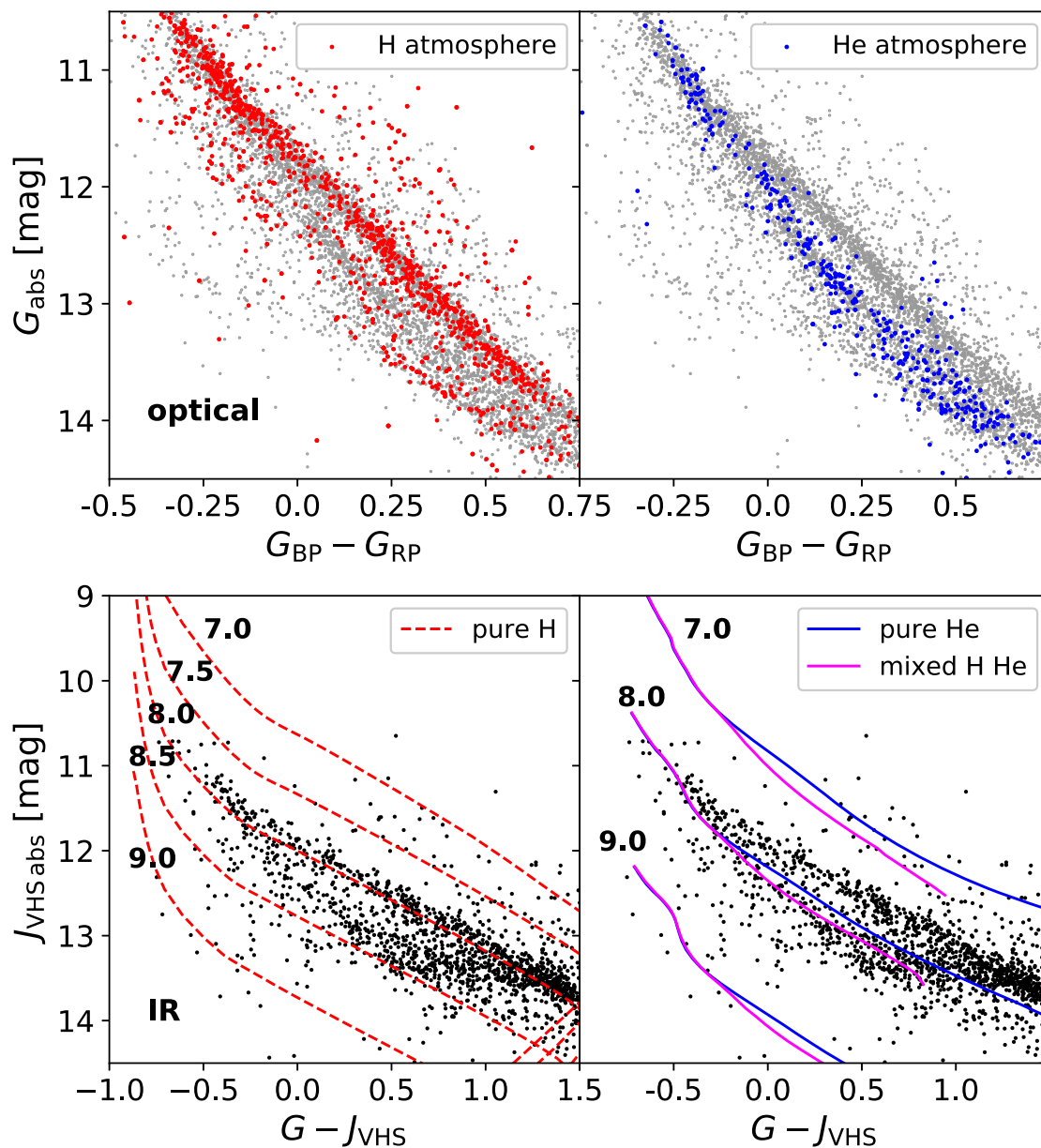
Figure 8. *Top panels:* H–R diagrams showing the distribution of *Gaia* white dwarfs using optical colours. High-confidence white dwarf candidates within 50 pc of the Sun from Gentile Fusillo et al. (2019) are displayed in grey. To highlight the bifurcation between white dwarfs with different atmospheric composition, pure H and He-atmosphere white dwarfs identified using Sloan Digital Sky Survey (SDSS) spectroscopy are shown in red (top left) and blue (top right), respectively. *Bottom panels:* Distribution in the H–R diagram of white dwarfs within 50 pc of the Sun with available VHS *J*-band photometry. The bifurcation between pure H and He-rich atmosphere white dwarfs is clearly visible also in IR colours for $G - J_{VHS} \gtrsim -0.25$. *Bottom left panel:* cooling tracks for pure H atmosphere white dwarfs at different log *g* values are displayed in red showing a good agreement between the predicted log $g \approx 8.0$ value and observed IR fluxes for DA white dwarfs in the upper luminous branch of the bifurcation. *Right-hand panel:* cooling tracks for pure He and mixed (H/He = 10^{-5} by number) atmosphere white dwarfs at different log *g* values are displayed in blue and magenta, respectively. Pure He models (blue) at a log $g \approx 8.0$ value clearly fail to reproduce the observed IR fluxes in the lower branch of the bifurcation while the mixed models (magenta) achieve a better agreement. Mixed atmosphere tracks have been truncated at $T_{eff} = 5000$ K, below which they strongly differ from the observations.

white dwarfs is clearly visible even at IR wavelengths (Fig. 8). Analogously to what we showed for the optical H–R diagram in Gentile Fusillo et al. (2019), Fig. 8 also illustrates that while the DA cooling track can be modelled well, pure He model atmospheres do not correctly reproduce the cooling sequence of the He-atmosphere lower branch. Mixed model atmospheres with H/He = 10^{-5} in number result in a better agreement with the observed IR data in Fig. 8, similarly to what was demonstrated for the optical H–R diagram in Bergeron et al. (2019).

Below $T_{eff} = 5000$ K, the effect of collision-induced absorption predicted by our mixed models is far too strong leading to a marked discrepancy with the observed data. More recent models described in Blouin et al. (2019) appear to have solved this low-temperature discrepancy by including non-ideal ionization. A better comparison with IR photometry of low-temperature He-atmosphere white dwarfs may be possible once the predicted colours of these new model grids become available. None the less, the need to include additional degrees of freedom (H abundance and/or metals),

when modelling He-atmosphere white dwarfs, makes them more challenging to characterize, and so less suitable as calibrators than the more common DA stars.

5 CONCLUSION

We have conducted a pilot test of the reliability of intermediate temperature and cool white dwarfs ($T_{\rm eff} < 20\,000$ K) as calibrators, specifically in the IR regime. We have analysed newly acquired STIS + WFC3 *HST* spectrophotometry of the two bright white dwarfs WD1327−083 and WD2341+322 and find that current atmosphere and interior models correctly predict the observed fluxes of both objects within 3 per cent over the entire wavelength range from 1500 to 17 000 Å. We therefore conclude that intermediate temperature white dwarfs are fully consistent with the *HST* flux scale and, in most cases, could be used as calibrators that are equally reliable as the current hot primary standards. The synthetic spectra which best match the STIS + WFC3 SED of WD1327−083 and WD2341+322 are available with the electronic distribution of this article. The much higher space density of cooler white dwarfs, $\simeq 4\,\mathrm{deg}^{-2}$ compared to a value of $\simeq 0.75\,\mathrm{deg}^{-2}$ for their hot counterparts, represents a significant advantage when looking for suitable calibrators for both large surveys and single observations. Additionally, since the SED of cool white dwarfs peaks much closer to the near-IR compared to the hot flux standards, these objects will be better suited as calibrators for the observations conducted by the next-generation IR facilities like *Euclid* and *JWST*.

To reliably test the robustness of white dwarf models in the IR regime we ran two additional experiments: a model fit to the Paschen line profiles and a comparison with IR photometric observations. For the Paschen line fits, we have developed a technique analogous to the well-established Balmer line spectroscopic method and vetted its reliability using a small sample of H-atmosphere white dwarfs observed with the X-shooter spectrograph on the VLT. We have then fitted the Paschen line profiles to obtain stellar parameters that only rely on near-IR spectroscopic data. For all stars, we find $T_{\rm eff}$ and log g values in close agreement with those obtained from the analysis of their optical and UV spectra. This opens up a new venue of analysis for white dwarfs in the near-IR regime. For the second test, we have compared the optical versus IR colour–colour diagrams computed from our white dwarf models with the observed distribution of these objects within 50 pc as observed by *Gaia*, 2MASS, UKIDSS, VHS, and *WISE*. We show that the model tracks closely match the observations for all surveys. While the implication of these results depends on our understanding of the calibration of these surveys, this suggests that our models adequately predict IR fluxes of cool white dwarfs.

REFERENCES

Becklin E. E., Farihi J., Jura M., Song I., Weinberger A. J., Zuckerman B., 2005, ApJ, 632, L119

Bergeron P., Saffer R. A., Liebert J., 1992, ApJ, 394, 228

Bergeron P., Leggett S. K., Ruiz M. T., 2001, ApJS, 133, 413

Bergeron P., Dufour P., Fontaine G., Coutu S., Blouin S., Genest-Beaulieu C., Bédard A., Rolland B., 2019, ApJ, 876, 67

Blouin S., Dufour P., Thibeault C., Allard N. F., 2019, ApJ, 878, 63

Bohlin R. C., 2014, AJ, 147, 127

Bohlin R. C., Deustua S. E., 2019, AJ, 157, 229

Bohlin R., Deusua S. E., de Rosa G., 2019, AJ, 158, 211

Bohlin R. C., Gordon K. D., Tremblay P.-E., 2014, PASP, 126, 711

Bohlin R., Deustua S. E., Pirzkal N., 2015, Technical Report, IR Grism Wavelength Solutions Using the Zero Order Image as the Reference Point

Brink"worth C. S., Burleigh M. R., Lawrie K., Marsh T. R., Knigge C., 2013, ApJ, 773, 47

Chambers K. C. et al., 2016, preprint (arXiv:1612.05560)

Evans D. W. et al., 2018, A&A, 616, A4

Fontaine G., Brassard P., Bergeron P., 2001, PASP, 113, 409

Freudling W., Romaniello M., Bramich D. M., Ballester P., Forchi V., García-Dabló C. E., Moehler S., Neeser M. J., 2013, A&A, 559, A96

Gaia Collaboration, 2018, A&A, 616, A1

Genest-Beaulieu C., Bergeron P., 2019, ApJ, 871, 169

Gentile Fusillo N. P. et al., 2019, MNRAS, 482, 4570

Giannias A., Bergeron P., Dupuis J., Ruiz M. T., 2010, ApJ, 720, 581

Giannias A., Bergeron P., Ruiz M. T., 2011, ApJ, 743, 138

Gomez T. A., Nagayama T., Kilcrease D. P., Montgomery M. H., Winget D. E., 2016, Phys. Rev. A, 94, 022501

Holberg J. B., Bergeron P., 2006, AJ, 132, 1221

Hounsell R. et al., 2018, ApJ, 867, 23

Hubeny I., Lanz T., 1995, ApJ, 439, 875

Hummer D. G., Mihalas D., 1988, ApJ, 331, 794

Kalirai J., 2018, Contemp. Phys., 59, 251

Koester D., 2010, Mem. Soc. Astron. Ital., 81, 921

Koester D., Schulz H., Weidemann V., 1979, A&A, 76, 262

Lawrence A. et al., 2007, MNRAS, 379, 1599

Liebert J., Bergeron P., Holberg J. B., 2005, ApJS, 156, 47

Marsh T. R., Dhillon V. S., Duck S. R., 1995, MNRAS, 275, 828

McMahon R. G., Banerji M., Gonzalez E., Koposov S. E., Bejar V. J., Lodieu N., Rebolo R., VHS Collaboration, 2013, Messenger, 154, 35

Narayan G. et al., 2019, ApJS, 241, 20

Padmanabhan N. et al., 2008, ApJ, 674, 1217

Perlmutter S. et al., 1999, ApJ, 517, 565

Preval S. P., Barstow M. A., Badnell N. R., Holberg J. B., Hubeny I., 2015, in Dufour P., Bergeron P., Fontaine G., eds, ASP Conf. Ser. Vol. 493, 19th European Workshop on White Dwarfs. Astron. Soc. Pac., San Francisco, p. 15

Racca G. D. et al., 2016, in MacEwen H. A., Fazio G. G., Lystrup M., Batalha N., Siegler N., Tong E. C., eds, Proc. SPIE Conf. Ser. Vol. 9904, Space Telescopes and Instrumentation 2016: Optical, Infrared, and Millimeter Wave. SPIE, Bellingham, p. 99040O

Riess A. G. et al., 1998, AJ, 116, 1009

Riess A. G. et al., 2000, ApJ, 536, 62

Scolnic D. et al., 2014, ApJ, 795, 45

Skrutskie M. F. et al., 2006, AJ, 131, 1163

Smette A. et al., 2015, A&A, 576, A77

Taylor M. B., 2005, in Shopbell P., Britton M., Ebert R., eds, ASP Conf. Ser. Vol. 347, Astronomical Data Analysis Software and Systems XIV. Astron. Soc. Pac., San Francisco, p. 29

Thatte N. A. et al., 2016, in Evans C. J., Simard L., Takami H., eds Proc. SPIE Conf. Ser. Vol. 9908, Ground-based and Airborne Instrumentation for Astronomy VI. SPIE, Bellingham, p. 99081X

Tremblay P.-E., Bergeron P., 2009, ApJ, 696, 1755

Tremblay P.-E., Bergeron P., Gianninas A., 2011, ApJ, 730, 128

Tremblay P.-E., Ludwig H.-G., Steffen M., Freytag B., 2013, A&A, 559, A104

Tremblay P.-E., Gianninas A., Kilic M., Ludwig H.-G., Steffen M., Freytag B., Hermes J. J., 2015, ApJ, 809, 148

Tremblay P.-E. et al., 2017, MNRAS, 465, 2849

Tremblay P.-E., Cukanovaite E., Gentile Fusillo N. P., Cunningham T., Hollands M. A., 2019, MNRAS, 482, 5222

Vernet J. et al., 2011, A&A, 536, A105

Wright E. L. et al., 2010, AJ, 140, 1868

SUPPORTING INFORMATION

Supplementary data are available at *MNRAS* online.

WD2341+322_model.dat
WD1327-083_model.dat

Please note: Oxford University Press is not responsible for the content or functionality of any supporting materials supplied by the authors. Any queries (other than missing material) should be directed to the corresponding author for the article.

APPENDIX A: OBSERVATION LOG

Table A1. Log of *HST* observations.

Object	Telescope/instrument	Grating	Exposure time (s)	Date (yyyy-mm-dd)
WD1327−083	HST/STIS	G750L	936.0	2016-4-15
	HST/STIS	G430L	200.0	2016-4-15
	HST/STIS	G230L	605.0	2016-4-15
	HST/STIS	G140L	1244.0	2016-4-15
	HST/WFC3	G141	60.14	2016-4-15
	HST/WFC3	G102	83.51	2016-4-15
WD2341+322	HST/STIS	G750L	939.0	2016-5-27
	HST/STIS	G430L	240.0	2016-5-27
	HST/STIS	G230L	650.0	2016-5-27
	HST/STIS	G140L	1370.0	2016-5-27
	HST/WFC3	G141	128.45	2016-5-27
	HST/WFC3	G102	175.98	2016-5-27

This paper has been typeset from a TeX/LaTeX file prepared by the author.